SIAM J. APPL. MATH.
Vol. 48, No. 5, October 1988

003

THE RIEMANN PROBLEM NEAR A HYPERBOLIC SINGULARITY: THE CLASSIFICATION OF SOLUTIONS OF QUADRATIC RIEMANN PROBLEMS I*

E. ISAACSON†, D. MARCHESIN‡, B. PLOHR§, AND B. TEMPLE¶

Abstract. The purpose of this paper is to classify the solutions of Riemann problems near a hyperbolic singularity in a nonlinear system of conservation laws. Hyperbolic singularities play the role in the theory of Riemann problems that rest points play in the theory of ordinary differential equations: Indeed, generically, only a finite number of structures can appear in a neighborhood of such a singularity. In this, the first of three papers, the program of classification is discussed in general and the simplest structure that occurs is characterized.

Key words. nonlinear hyperbolic conservation laws, Riemann problems, hyperbolic singularities

AMS(MOS) subject classifications. 35L65, 35L67, 35L80

Introduction. We study the Riemann problem for nonlinear 2×2 systems of conservation laws:

$$U_t + f(U)_x = 0, \tag{A}$$

$$U(x,0) = U_0(x) = \begin{cases} U_L, & x \leqq 0, \\ U_R, & x > 0. \end{cases} \tag{B}$$

Our purpose is to classify the structure of the wave curves and the solution of the Riemann problem in a neighborhood of an isolated point U_0 in state space where the wave speeds λ_1 and λ_2 coincide. Here λ_1, λ_2 are the eigenvalues of the matrix ∇f. We refer to such a point U_0 as an isolated hyperbolic singularity, or an umbilic point.

Such singularities play a role in the wave structure of solutions of the Riemann problem similar to the role of rest points in the theory of ordinary differential equations. Indeed, the topological structure of the wave curves for (A), (B) are drastically altered in a neighborhood of a hyperbolic singularity in a fashion similar to the alteration of solution curves of ordinary differential equations in a neighborhood of a rest point.

* Received by the editors November 23, 1987; accepted for publication (in revised form) February 11, 1988. A preliminary version of this work appeared as PUC/RJ Report MAT 12-85.

† Department of Mathematics, University of Wyoming, Laramie, Wyoming 82071. This work was supported in part by National Science Foundation grant DMS-831229, Department of Energy contract DE-AC02-76ER03077, by the University of Wyoming Division of Basic Research, by Air Force Office of Scientific Research grant AFOSR-850117, and by CNPq/Brazil grant 403039/84-MA.

‡ Department of Mathematics, Pontificia Universidade Catolica do Rio de Janeiro, Rio de Janeiro, Brazil 22453. This work was supported in part by CNPq/Brazil fellowship 30.0204/83-MA, National Science Foundation grant DMS-831229, and Department of Energy contract DE-AC02-76ER03077.

§ Department of Computer Science and Mathematics Research Center, University of Wisconsin, Madison, Wisconsin 53705. This work was supported in part by National Science Foundation grant DMS-831229, Department of Energy contract DE-AC02-76ER03077, and the U.S. Army under contract DAAG29-80-C-0041. This material is based upon work supported by the National Science Foundation under grant DMS-8210950, Mod. 1.

¶ Department of Mathematics, University of California, Davis, California 95616. This work was supported in part by FINEP/Brazil grant 4.3.82.017.9, CNPq/Brazil grant 1.01.10.011/84-ACI, National Science Foundation grant 5274298INT-8415209, and the U.S. Army under contract DAAG-29-80-C-0041. This material is based upon work supported by the National Science Foundation under grant DMS-8210950, Mod. 1.

As with the case of rest points, there are generically only a finite number of structures that can appear near an isolated hyperbolic singularity, and it is our purpose to classify them.

Our method is to use a classification of integral curves proposed in [8] and carried out in [17]. This established four types of singularities, labeled I–IV, classified according to four distinct structures of the rarefaction curves near the singularity. In this paper we describe our general program for classifying the structure of the wave curves for solution of the Riemann problem near hyperbolic singularities, and we construct these solutions for the type of singularity that exhibits the simplest structure, namely the symmetric cases of type IV. Our analysis uses a numerical determination of the Hugoniot locus. Similar constructions for singularities of types II and III will follow. A particular solution of type I was presented in [18].

Our method is to approximate the flux function f near the singularity by a quadratic flux function. The structure of the singularity is then determined by the coefficients in the quadratic approximations. We discuss this in detail in the next section, and we present the structure of the wave curves and the solution of the Riemann problem (A), (B) for the values of these parameters corresponding to the symmetric systems with a singularity of type IV.

Remarkable features arise in singularities of type IV: the integral curves do not form a coordinate system in a neighborhood of the singularity; the Hugoniot loci generally form loops; the classical shocks lie on disconnected portions of the Hugoniot locus; waves curves end; and the qualitative structure of the wave curves changes drastically as the base point U_L crosses certain critical lines. Even so, the Riemann problem is solved everywhere within the class of classical shocks and rarefaction waves, and solutions depend continuously on U_L and U_R. Additional features appear for singularities of types II and III.

1. Preliminaries. We consider the general 2×2 system of conservation laws with quadratic flux functions

$$\begin{aligned} &u_t+\tfrac{1}{2}\{a_1u^2+2b_1uv+c_1v^2\}_x=0,\\ &v_t+\tfrac{1}{2}\{a_2u^2+2b_2uv+c_2v^2\}_x=0. \end{aligned} \tag{1}$$

In particular, we solve the Riemann problem globally for a specific range of the coefficients a_i, b_i, c_i.

System (1) is of interest because solutions of (1) approximate solutions of an arbitrary 2×2 system of conservation laws

$$\mathbf{u}_t+\mathbf{f}(\mathbf{u})_x=\mathbf{0}, \tag{2}$$

where $\mathbf{u}=(u, v)$, $\mathbf{f}=(f, g)$, in a neighborhood of an isolated hyperbolic singularity. Such a singularity is an isolated point in a neighborhood of which (2) is hyperbolic and at which the Jacobian

$$A(\mathbf{u})\equiv\frac{\partial\mathbf{f}}{\partial\mathbf{u}}=\begin{bmatrix} f_u & f_v\\ g_u & g_v\end{bmatrix}$$

has equal eigenvalues and is diagonalizable. In fact, system (1) is obtained from system (2) as follows. Let $\lambda_1(\mathbf{u})\leqq\lambda_2(\mathbf{u})$ denote the eigenvalues of $A(\mathbf{u})$, and let $\mathbf{u}_0$ denote the isolated point at which $\lambda_1(\mathbf{u}_0)=\lambda_2(\mathbf{u}_0)\equiv\lambda_0$. First, replace $\mathbf{u}$ by $\mathbf{u}-\mathbf{u}_0$ and translate the reference frame (x, t) to $(x-\lambda_0t, t)$ so that the resulting system has an isolated singularity at $\mathbf{u}=(0, 0)$ with corresponding double eigenvalue $\lambda=0$. Then system (1)

is obtained by expanding the flux functions of this transformed system in Taylor series about (0, 0) and neglecting higher-order terms.

System (1) can be reduced further by a nonsingular linear change of dependent variables. Two systems related by such a transformation S are isomorphic in the sense that $S\mathbf{u}(x, t)$ is a weak solution of the transformed system if and only if $\mathbf{u}(x, t)$ is a weak solution of the original system. Since the nonsingular transformation S contains four free parameters and since system (1) contains six parameters, we expect to find a two-parameter family of isomorphism classes for system (1). Thus, we look for representatives of the isomorphism classes in a normal form containing two free parameters [8]. In [17] it was shown that when system (1) is hyperbolic, there is a nonsingular linear change of dependent variables that transforms system (1) into

$$\begin{aligned} &u_t+\tfrac{1}{2}\{au^2+2buv+v^2\}_x=0,\\ &v_t+\tfrac{1}{2}\{bu^2+2uv\}_x=0. \end{aligned} \tag{3}$$

System (3) depends on two free parameters a and b and can be taken as a normal form for the hyperbolic quadratic systems (1). It is also shown in [3], [17] that the integral curves of (3) fall into four nonisomorphic classes depending on the parameters a and b. These classes define four regions in the a, b-plane referred to as Regions I–IV.

The regions are determined by the number of lines that form the Hugoniot locus of the origin, as well as the direction of increase of the appropriate eigenvalue on these lines. In Regions I–III, the Hugoniot locus consists of three distinct lines, while in Region IV it consists of one line. Specifically, the boundary between Regions I and II is given by $a=\frac{3}{4}b^2$; the boundary between Regions II and III is given by $a=1+b^2$; and the boundary between Regions III and IV is given by $4\{4b^2-3(a-2)\}^3=\{16b^3+9(1-2a)b\}^2$ (cf. [17]). The structure of solutions in each region is simplest when $b=0$ since then solutions have both up-down symmetry ($(u, -v)$ satisfies (3) if and only if (u, v) does) and left-right symmetry ($(u(x, t), v(x, t))$ satisfies (3) if and only if $(-u(-x, t), v(-x, t))$ does). We call the systems with $b=0$ symmetric. (An additional simplifying feature of the symmetric systems is that the lines on which genuine nonlinearity fails coincide with the Hugoniot locus of the origin.)

The present paper is the first of a series in which we give the solution of the Riemann problem:

$$\mathbf{u}(x, 0)=\begin{cases}\mathbf{u}_L\equiv(u_L, v_L), & x<0,\\ \mathbf{u}_R\equiv(u_R, v_R), & x\geqq 0\end{cases} \tag{4}$$

for the symmetric systems in Regions II–IV of [17]. There are new features in these regions that do not occur in Region I (cf. [18]). First, a type of shock we call compressive appears in solutions of the Riemann problem, and the existence of such shocks is necessary to ensure (in the x, t-plane) the continuous dependence of solutions on $\mathbf{u}_L$ and $\mathbf{u}_R$ (cf. [6], [7], [9], [21]). In [25] it is noted that the compressive shocks perturb to a one-shock followed by a two-shock. This fact is manifested in the triple shocks that appear in the solutions.

A second feature that occurs in Regions II–IV that does not occur in Region I is the following: in Regions II–IV there are lines on which $\lambda=0$, whereas in Region I, $\lambda=0$ if and only if $\mathbf{u}=0$. These lines play a central role both in the classification as well as in the structure of Riemann problem solutions. In fact, the lines $\lambda=0$ give a geometric interpretation for the boundaries between the Regions I–III located in [17]. (See the Appendix and Fig. 8.) Also, in Regions II–IV the structure of the shock types on the Hugoniot locus of a point $\mathbf{u}$ changes as $\mathbf{u}$ crosses a line $\lambda=0$; this entails a

corresponding change in the structure of the solutions of the Riemann problem. The reason for the change in shock type is that the state $\mathbf{u}$ on the line $\lambda = 0$ can be joined to the state $-\mathbf{u}$ by a two-sided contact discontinuity.

Our construction of the solutions of the Riemann problem is based on a numerical construction of the Hugoniot loci together with the structure of the integral curves obtained from [17]. Some analysis is presented to justify the salient features of the solutions obtained. In particular, our analysis uses an explicit parameterization of the Hugoniot locus (see the Appendix). The fact that the Hugoniot locus is star-like with respect to the left state was pointed out in [24].

In the present paper we give the solution of the Riemann problem for system (3) in the parameter range

$$a > 2, \qquad b = 0. \tag{5}$$

This condition specifies the symmetric systems in Region IV. We present the solution in § 3 by means of a series of diagrams (Fig. 7(a)-(f)). Because of up-down symmetry, we give the solutions only for $\mathbf{u}_L$ in the lower half-plane. The solution diagrams are qualitatively the same for all $\mathbf{u}_L$ in the sector

$$\mathcal{A}_1 = \{\mathbf{u}\colon \theta_* < \theta_L < 0\},$$

and are qualitatively the same for all $\mathbf{u}_L$ in the sector

$$\mathcal{A}_2 = \{\mathbf{u}\colon -\pi < \theta_L < \theta_*\}$$

(see Fig. 2); here

$$\theta_L = \arctan\left(\frac{v_L}{u_L}\right), \qquad \theta_* = \arctan\left(-\sqrt{a}\right).$$

This separation angle θ_* depends on a, and the ray $\theta = \theta_*$ is the ray (in the lower half-plane) on which $\lambda_1 = 0$. The solution consists of a one-composite wave followed by a two-composite wave in analogy with the local solutions for strictly hyperbolic systems (cf. [11], [14]). Here, however, the wave curves have a different structure: as in [6], [7], [9], [21], intermediate solution states do not depend continuously on the data due to the appearance of compressive shocks. However, as in [6], [7], [9], [21], continuous dependence on $\mathbf{u}_L$ and $\mathbf{u}_R$ is ensured in x, t-space because of the coincidence of shock speeds in the compressive shocks. In this paper we construct explicitly for each state $\mathbf{u}$ the one-wave curve $\mathcal{W}_1(\mathbf{u})$ and the two-wave curve $\mathcal{W}_2(\mathbf{u})$ such that the following theorem holds.

THEOREM. *For each pair of states $\mathbf{u}_L$ and $\mathbf{u}_R$, there exists an intermediate state $\mathbf{u}_M \in \mathcal{W}_1(\mathbf{u}_L)$ such that $\mathbf{u}_R \in \mathcal{W}_2(\mathbf{u}_M)$ and the solution of the Riemann problem* (3), (4) *consists of the one-wave from $\mathbf{u}_L$ to $\mathbf{u}_M$ followed by the two-wave from $\mathbf{u}_M$ to $\mathbf{u}_R$. Moreover, the solution is unique in x, t-space and depends continuously on $\mathbf{u}_L$ and $\mathbf{u}_R$.*

In Fig. 7(a)-(f), pictorial solutions of the Riemann problem are presented in which the state $\mathbf{u}_L$ is fixed, and an arbitrary point in the diagram represents $\mathbf{u}_R$. The waves in the solution of the Riemann problem are determined by the path from $\mathbf{u}_L$ to $\mathbf{u}_R$, which consists of (portions of) wave curves and is indicated by arrows.

In § 2 we discuss the wave curves $\mathcal{W}_1$ and $\mathcal{W}_2$. In § 3 we describe the diagrams in Fig. 7(a)-(e) individually, and in § 4 we verify the salient features of these diagrams. General properties of system (1) are stated in the Appendix and are referred to throughout. The Appendix also contains the interpretation of Regions I-III in terms of the lines $\lambda = 0$. These are depicted in Fig. 8(a)-(d).

2. Elementary waves. The integral curves of the eigenvector fields of the Jacobian $A(\mathbf{u})$ determine the rarefaction waves of system (2). The Hugoniot loci $\mathscr{H}(\mathbf{u}_L)$ for states $\mathbf{u}_L$ determine the shock waves of system (2), and are given by [20]

$$\mathscr{H}(\mathbf{u}_L) \equiv \{\mathbf{u}\colon s(\mathbf{u}-\mathbf{u}_L) = \mathbf{f}(\mathbf{u}) - \mathbf{f}(\mathbf{u}_L) \text{ for some } s \in R\}.$$

The general solution of the Riemann problem we construct is obtained by composing rarefaction waves and shock waves. Because the flux functions in (1) are homogeneous quadratics, the integral curves and Hugoniot loci for system (1) have the following scaling property: if Γ is an integral curve or Hugoniot locus through $\mathbf{u}_L$, then $c\Gamma$ is the corresponding integral curve or Hugoniot locus through $c\mathbf{u}_L$, $c \neq 0$. The eigenvalues and shock speeds scale similarly. Thus the integral curves and Hugoniot locus through $\mathbf{u}_L$ determine the corresponding integral curves and Hugoniot locus for each state $\mathbf{u}$ satisfying $\theta = \theta_L$ where

$$\theta = \arctan\left(\frac{v}{u}\right).$$

For the Hugoniot loci, the up-down and left-right symmetries imply that if $\mathbf{u}_R \in \mathscr{H}(\mathbf{u}_L)$, then $\bar{\mathbf{u}}_R \in \mathscr{H}(\bar{\mathbf{u}}_L)$ and $\hat{\mathbf{u}}_R \in \mathscr{H}(\hat{\mathbf{u}}_L)$ where $\bar{\mathbf{u}} = (u, -v)$ and $\hat{\mathbf{u}} = (-u, v)$. Thus, the reflection of a Hugoniot curve about either the u- or v-axis is also a Hugoniot curve. In terms of wave speeds and shock speeds, the symmetries of (3) when $b = 0$ yield the following relationships:

$$\lambda_p(\mathbf{u}) = \lambda_p(\bar{\mathbf{u}}) = -\lambda_{\hat{p}}(\hat{\mathbf{u}}), \qquad p = 1, 2, \tag{2.1}$$

$$\sigma(\mathbf{u}_L, \mathbf{u}_R) = \sigma(\bar{\mathbf{u}}_L, \bar{\mathbf{u}}_R) = \sigma(\hat{\mathbf{u}}_L, \hat{\mathbf{u}}_R) \tag{2.2}$$

where $\hat{p}$ denotes the other family, and σ denotes shock speed.

In Table 1 we label nine types of shocks according to the inequalities that hold between the characteristic speeds of $\mathbf{u}_L, \mathbf{u}_R$ and the shock speed $\sigma(\mathbf{u}_L, \mathbf{u}_R)$. (Obvious inequalities are omitted.) Since the two wave speeds λ_1 and λ_2 assigned to each state are ordered, Table 1 gives the totality of shock types that can occur in any 2×2 system (2). In the case of the symmetric systems (3), the formulas (2.1) and (2.2) imply the following symmetries for shock types: if $\mathbf{u}_R \in \mathscr{H}(\mathbf{u}_L)$, then the shock type of $\langle \bar{\mathbf{u}}_L, \bar{\mathbf{u}}_R \rangle$ will be the same as the shock type of $\langle \mathbf{u}_L, \mathbf{u}_R \rangle$; and the shock type of $\langle \hat{\mathbf{u}}_L, \hat{\mathbf{u}}_R \rangle$ will be what we call the inverse of the shock type of $\langle \mathbf{u}_L, \mathbf{u}_R \rangle$. Here, the inverse shock type is obtained by reversing the inequalities that hold between the shock speed and each wave speed to the right and left of the shock and also by interchanging the families one and two. Therefore (cf. Table 1), one-shock and two-expansive are inverses; two-shock and one-expansive are inverses; compressive and expansive are inverses; right transport and left transport are inverses; and crossing is its own inverse. Thus in the symmetric cases, all Hugoniot curves and shock types are determined by the Hugoniot curves and shock types for states in a single quadrant of the u, v-plane. Among the above shock types, some occur in the solutions of system (3) that do not occur for strictly hyperbolic systems. For the symmetric systems of classes II–IV, there are three types of shocks that appear in solutions: one-shocks, two-shocks, and compressive shocks defined by (cf. Table 1)

$$\lambda_1(\mathbf{u}_R) \leqq \lambda_2(\mathbf{u}_R) \leqq \sigma(\mathbf{u}_L, \mathbf{u}_R) \leqq \lambda_1(\mathbf{u}_L) \leqq \lambda_2(\mathbf{u}_L).$$

We refer to any of the three types of shocks described above as admissible. We refer to shocks of other types as inadmissible. (We note that the transport shocks are the only types that do not appear in Hugoniot loci of the symmetric systems in classes II–IV.) Our scheme for labeling shock types in Figs. 3–7 is described in Table 2.

TABLE 1

In the diagrams below, the centerline denotes a shock in x, t-space. The lines to the left and right of the shock are characteristic lines, and indicate the relationship between the shock speed and the wave speeds on the left and right.

One-shock:	$s < \lambda_1(\mathbf{u}_L)$ $\lambda_1(\mathbf{u}_R) < s < \lambda_2(\mathbf{u}_R)$	
One-expansive:	$\lambda_1(\mathbf{u}_L) < s < \lambda_2(\mathbf{u}_L)$ $s < \lambda_1(\mathbf{u}_R)$	
Two-shock:	$\lambda_1(\mathbf{u}_L) < s < \lambda_2(\mathbf{u}_L)$ $\lambda_2(\mathbf{u}_R) < s$	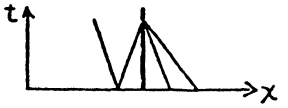
Two-expansive:	$\lambda_2(\mathbf{u}_L) < s$ $\lambda_1(\mathbf{u}_R) < s < \lambda_2(\mathbf{u}_R)$	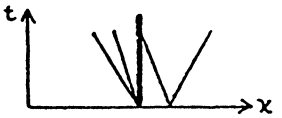
Compressive:	$\lambda_2(\mathbf{u}_R) < s < \lambda_1(\mathbf{u}_L)$	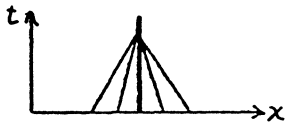
Expansive:	$\lambda_2(\mathbf{u}_L) < s < \lambda_1(\mathbf{u}_R)$	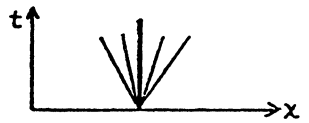
Crossing:	$\lambda_1(\mathbf{u}_L) < s < \lambda_2(\mathbf{u}_L)$ $\lambda_1(\mathbf{u}_R) < s < \lambda_2(\mathbf{u}_R)$	
Right transport:	$s < \lambda_1(\mathbf{u}_L)$ $s < \lambda_1(\mathbf{u}_R)$	
Left transport:	$\lambda_2(\mathbf{u}_L) < s$ $\lambda_2(\mathbf{u}_R) < s$	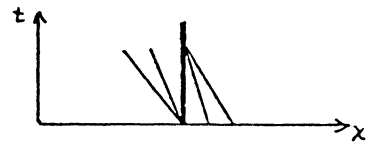

2.1. Integral curves. For system (3) with parameter values (5),

$$A(\mathbf{u}) = \begin{bmatrix} au & v \\ v & u \end{bmatrix},$$

and the integral curves are depicted in Fig. 1 [3], [17]. We call the integral curves associated with the eigenvalues $\lambda_1(\mathbf{u}) \leqq \lambda_2(\mathbf{u})$ the one-, two-integral curves. For example, when $a = 3$ the integral curves are the one-parameter family of parabolas

$$u - u_0 = -\frac{1}{4u_0} v^2,$$

where u_0 is the value at which the parabola crosses the u-axis. The u-axis is itself an integral curve for the symmetric systems $b = 0$. For general $a > 2$, the integral curves are parabola-like and the one-integral curves open to the left, the two-integral curves open to the right. The arrows in Fig. 1 indicate the direction in which the corresponding

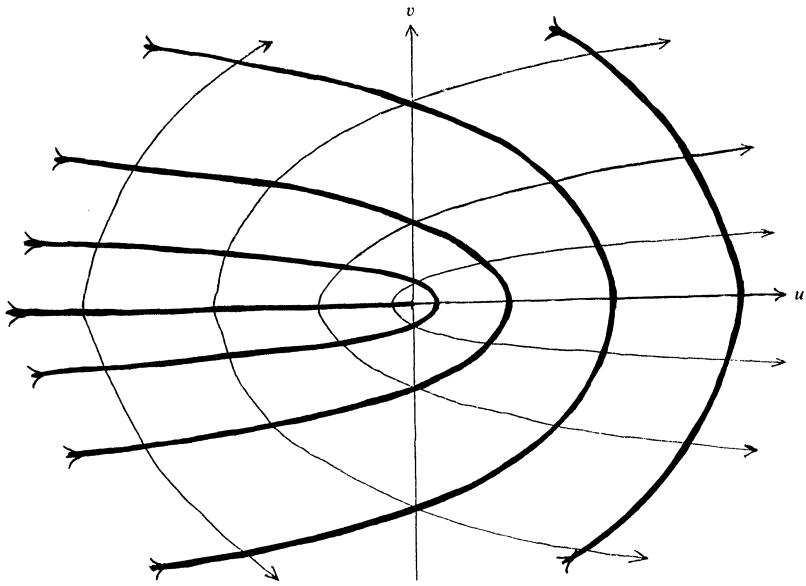

FIG. 1. *Integral curves for the symmetric systems in Region* IV; *i.e., system* (3) *with* $b = 0$, $a > 2$. (*Family one is denoted by the thicker lines.*)

eigenvalues increase. We define the i-rarefaction curve $\mathscr{R}_i(\mathbf{u}_L)$, $i = 1, 2$, to be the set of states $\mathbf{u}_R$ such that the solution of the Riemann problem (3), (4) is a pure i-rarefaction wave (see [14]); $\mathscr{R}_i(\mathbf{u}_L)$ is thus the connected portion of the i-integral curve through $\mathbf{u}_L$ consisting of those states $\mathbf{u}$ for which λ_i increases along the curve from $\mathbf{u}_L$ to $\mathbf{u}$.

2.2. The Hugoniot locus. For system (3) with parameter values (5), the qualitative shape of the Hugoniot locus $\mathscr{H}(\mathbf{u}_L)$ is as follows: for $\mathbf{u}_L = \mathbf{0}$, $\mathscr{H}(\mathbf{u}_L)$ is the u-axis; for $\mathbf{u}_L$ on the u-axis, $\mathscr{H}(\mathbf{u}_L)$ consists of an ellipse together with the u-axis; and for $\mathbf{u}_L$ off the u-axis, $\mathscr{H}(\mathbf{u}_L)$ perturbs to a closed loop surrounding the origin with two tails that are asymptotic at infinity to opposite ends of the horizontal line

$$v = \frac{a}{a-2} v_L.$$

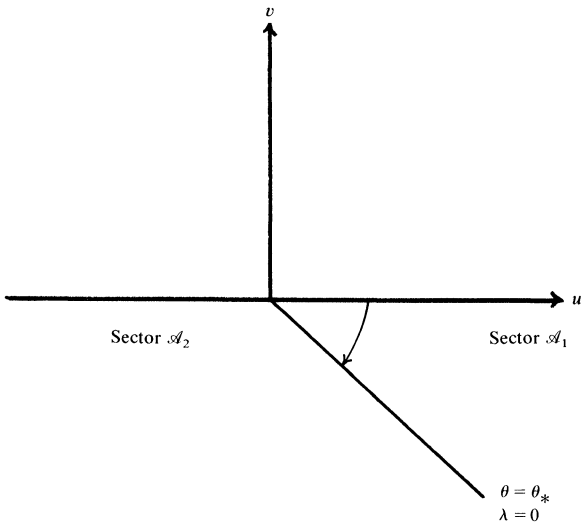

FIG. 2. *The Sectors $\mathscr{A}_1$, $\mathscr{A}_2$ determined by the ray $\theta = \theta_*$ ($\lambda_1 = 0$).*

These properties follow from the explicit parameterization of the Hugoniot locus given in the Appendix and are depicted in Fig. 3(a)-(f). The shock type is also indicated according to the notation in Table 2. We let $\mathscr{S}_p(\mathbf{u}_L)$ denote that portion of $\mathscr{H}(\mathbf{u}_L)$ consisting of one-shock for $p = 1$, two-shocks for $p = 2$, and compressive shocks for $p = c$.

The subset $\mathscr{S}_c(\mathbf{u}_L)$ is nonempty for $\mathbf{u}_L$ in the sector $\mathscr{A}_1$, and $\mathscr{S}_c(\mathbf{u}_L)$ is empty for $\mathbf{u}_L$ in the sector $\mathscr{A}_2$. Moreover, $\mathscr{S}_1(\mathbf{u}_L)$ has two disconnected components for $\mathbf{u}_L \in \mathscr{A}_1$ but only one for $\mathbf{u}_L \in \mathscr{A}_2$. This explains why the ray $\theta = \theta_*$ is the boundary across which the qualitative structure of the solution diagrams changes.

We note in Fig. 3(b) that B_L, D_L are the points at which

$$\sigma(\mathbf{u}_L, B_L) = \lambda_1(\mathbf{u}_L) = \sigma(\mathbf{u}_L, D_L);$$

in Fig. 3(a)-(d) that C_L is the point at which

$$\lambda_2(C_L) = \sigma(\mathbf{u}_L, C_L);$$

and in Fig. 3(c) that

$$\lambda_1(\mathbf{u}_L) = \sigma(\mathbf{u}_L, C_L) = \lambda_2(C_L)(=0).$$

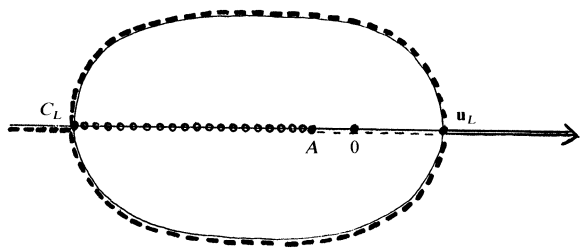

FIG. 3(a). *Hugoniot loci and shock types for $\mathbf{u}_L$ in representative positions.*

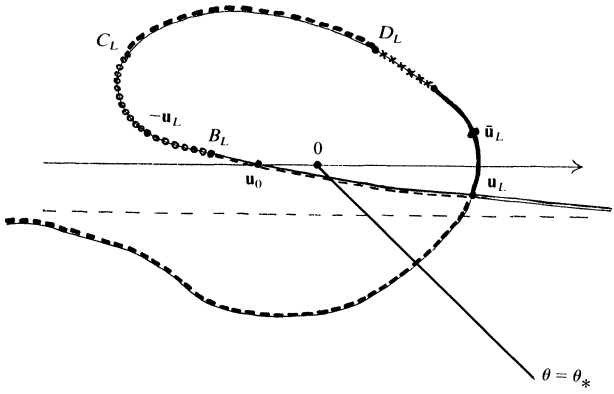

FIG. 3(b). *Hugoniot loci and shock types for* $\mathbf{u}_L$ *in representative positions.*

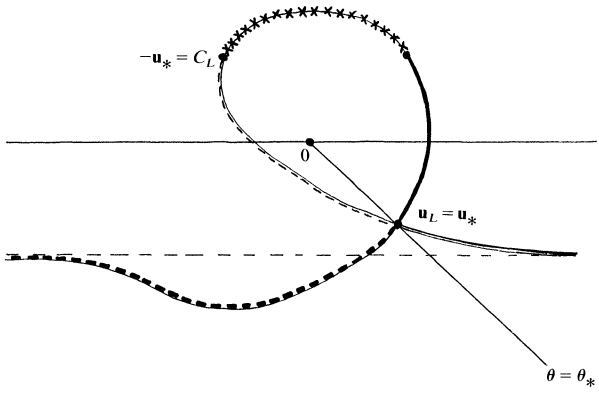

FIG. 3(c). *Hugoniot loci and shock types for* $\mathbf{u}_L$ *in representative positions.*

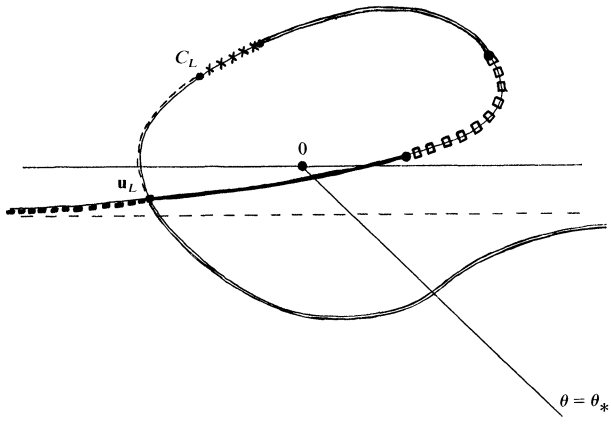

FIG. 3(d). *Hugoniot loci and shock types for* $\mathbf{u}_L$ *in representative positions.*

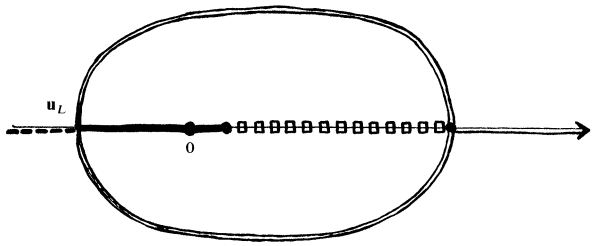

FIG. 3(e). *Hugoniot loci and shock types for* $\mathbf{u}_L$ *in representative positions.*

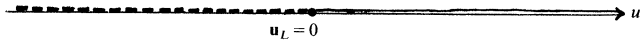

FIG. 3(f). *Hugoniot loci and shock types for* $\mathbf{u}_L$ *in representative positions.*

TABLE 2
Legend for Figs. 3–7.

	One-rarefaction
	One-expansive shock
	One-shock
	Two-rarefaction
	Two-expansive shock
	Two-shock (with or without arrows)
	One-composite (rarefaction followed by shock at characteristic speed)
	Compressive shock
	Crossing shock
	Expansive shock
	Two-boundary, triple shock curves
	Hugoniot locus of $\mathbf{u}_L$ and u-axis

Note 1. Arrows on rarefaction curves indicate the direction of increasing eigenvalue. Arrows on shock curves indicate the direction of decreasing shock speed.

Note 2. One- and two-shocks in the Hugoniot locus of $\mathbf{u}_L$ are indicated by dashed lines supported by the solid line for the Hugoniot locus.

2.3. Composite waves. The solutions of the Riemann problem are compositions of pure rarefaction waves and pure shock waves. We refer to a Riemann problem solution consisting entirely of waves of one family as a composite wave of that family. The composite waves in the solutions of Riemann problems for system (3) in parameter range (5) are of two types: a one-rarefaction wave followed by a one-shock wave and

a two-shock wave followed by a two-rarefaction wave. In each case, the speed of the shock equals the speed of the adjacent rarefaction wave. We call these one-*RS*- and two-*SR*-composite waves, respectively. (See Fig. 4. The letters in Fig. 4 refer to states appearing in Fig. 5 where the composite waves may be viewed in state space.)

For each $\mathbf{u}$ we define the one-composite curve $\mathscr{C}_1(\mathbf{u})$. In Fig. 5 a one-*RS*-composite wave with left state $\mathbf{u}$ is a wave consisting of a one-rarefaction wave from $\mathbf{u}$ to $F \in \mathscr{R}_1(\mathbf{u})$ followed by a one-shock from F to $D \in \mathscr{S}_1(F)$ such that $\sigma(F, D) = \lambda_1(F)$. Such a shock exists if and only if F lies on that portion of $\mathscr{R}_1(\mathbf{u})$ in Sector $\mathscr{A}_1$. We define the

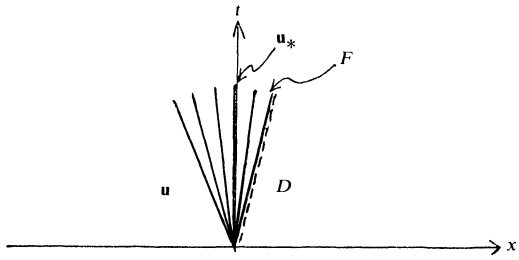

FIG. 4(a). *One-RS-composite wave in x, t-space.*

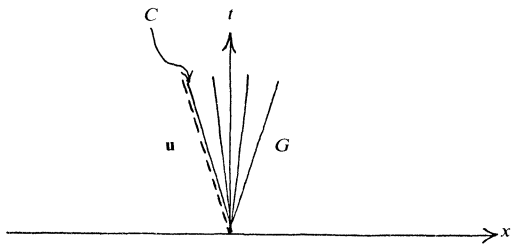

FIG. 4(b). *Two-SR-composite wave in x, t-space.*

one-composite curve $\mathscr{C}_1(\mathbf{u})$ to be the set of all such states D. Thus, the one-composite curve $\mathscr{C}_1(\mathbf{u}_*)$ is maximal for $\mathbf{u}_*$ on the boundary ray $\theta = \theta_*$ in the sense that

$$\mathscr{C}_1(\mathbf{u}_*) = \mathscr{C}_1(\mathbf{u}) \quad \text{for } \mathbf{u}_* \in \mathscr{R}_1(\mathbf{u}),$$

$$\mathscr{C}_1(\mathbf{u}_*) \supseteq \mathscr{C}_1(\mathbf{u}) \quad \text{for } \mathbf{u} \in \mathscr{R}_1(\mathbf{u}_*);$$

for example, in Fig. 5,

$$\mathscr{C}_1(\mathbf{u}) = \mathscr{C}_1(\mathbf{u}_*) = [EDC_*] \quad \text{and} \quad \mathscr{C}_1(F) = [ED] \subseteq \mathscr{C}_1(\mathbf{u}_*).$$

(Here, letters enclosed by brackets denote the curves that connect the corresponding points in the figures.) In fact, as F moves from E to $\mathbf{u}_*$ along $\mathscr{R}_1(\mathbf{u}_*)$, D moves from E to $\mathscr{C}_*$ along $\mathscr{C}_1(\mathbf{u}_*)$. Moreover,

$$C_* = -\mathbf{u}_*,$$

and

$$\sigma(\mathbf{u}_*, C_*) = \lambda_2(C_*) = \lambda_1(\mathbf{u}_*) = 0.$$

For each curve Γ we define the two-boundary curve based on Γ. In Fig. 5, a two-*SR*-composite wave with left state $\mathbf{u}$ is a wave consisting of a two-shock wave

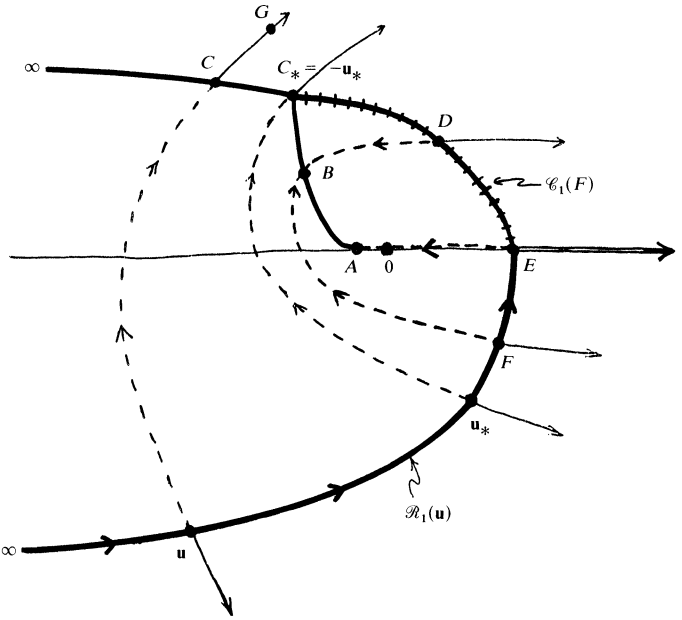

FIG. 5. *Typical curves*: *Rarefaction* ($\mathscr{R}_1(\mathbf{u}) = [\mathbf{u}FE]$); *One-composite* ($\mathscr{C}_1(F) = [ED]$); *Two-boundary* ($[\infty CC_*]$); *Triple shock* ($[ABC_*]$).

from $\mathbf{u}$ to $C \in \mathscr{S}_2(\mathbf{u})$ followed by a two-rarefaction wave from C to any $G \in \mathscr{R}_2(C)$ such that $\sigma(\mathbf{u}, C) = \lambda_2(C)$. Such a shock exists if and only if $\mathbf{u}$ lies on that portion of Γ in sector $\mathscr{A}_2$. We define the two boundary curve to be the set of all such states C. For example, in Fig. 5, $[C_*C^\infty]$ is the two-boundary curve based on $[\mathbf{u}_*\mathbf{u}^\infty]$. Thus, for left states $\mathbf{u}$ on $\Gamma = [\mathbf{u}_*\mathbf{u}^\infty]$, the states C on the two-boundary curve $[C_*C^\infty]$ are transition states between two-shock waves and two-composite waves.

2.4. Wave curves. We define the wave curve $\mathscr{W}_i(\mathbf{u}_L)$, $i = 1, 2$, to be the set of states $\mathbf{u}_R$ for which the solution of the Riemann problem (2), (4) is a pure composite wave of the appropriate family. Thus (see Fig. 6(a), (b)),

$$\mathscr{W}_1(\mathbf{u}_L) = \mathscr{S}_1(\mathbf{u}_L) \cup \mathscr{R}_1(\mathbf{u}_L) \cup \mathscr{C}_1(\mathbf{u}_L)$$

and

$$\mathscr{W}_2(\mathbf{u}_L) = \mathscr{R}_2(\mathbf{u}_L) \cup \mathscr{S}_2(\mathbf{u}_L) \cup \mathscr{R}_2(C),$$

where C is the endpoint of $\mathscr{S}_2(\mathbf{u}_L)$ at which $\sigma(\mathbf{u}_L, C) = \lambda_2(C)$. The geometry of these curves is indicated in Fig. 6 for $\mathbf{u}_L$ in Sectors $\mathscr{A}_1$ and $\mathscr{A}_2$.

3. Solution of the Riemann problem. For each $\mathbf{u}_L$ we describe the solution of the Riemann problem for arbitrary $\mathbf{u}_R$ by means of a diagram. In Fig. 7(b), (d) we present a diagram of the solution of the Riemann problem for representative values of $\mathbf{u}_L$ in Sectors $\mathscr{A}_1$ and $\mathscr{A}_2$ in each of which the solution diagrams are qualitatively the same. For completeness and in order to see clearly the continuous dependence of solutions on $\mathbf{u}_L$, we also give, in Fig. 7(a), (c), (e), the solution diagrams for typical values of $\mathbf{u}_L$ on the boundaries of Sectors $\mathscr{A}_1$ and $\mathscr{A}_2$, i.e., for $\mathbf{u}_L$ on the rays $\theta = 0$, $\theta = \theta_*$, and $\theta = -\pi$. In Fig. 7(a)-(d), the representative values $\mathbf{u}_L$ are chosen to lie

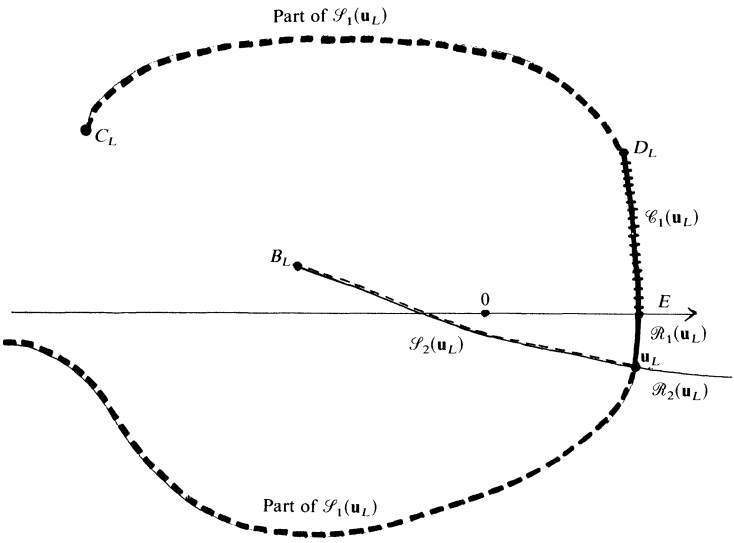

FIG. 6(a). *The wave curves for* $\mathbf{u}_L \in \mathscr{A}_1$.

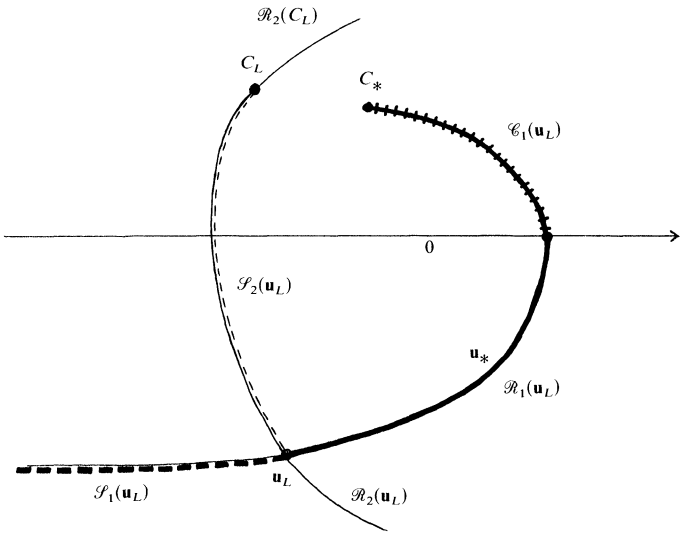

FIG. 6(b). *The wave curves for* $\mathbf{u}_L \in \mathscr{A}_2$.

on the one-integral curve through the fixed state E on the positive u-axis. In Fig. 7(f) we present the solution for $\mathbf{u}_L = \mathbf{0}$.

The solution of the Riemann problem consists of a one-wave with left state $\mathbf{u}_L$ and right state $\mathbf{u}_M$ followed by a two-wave with left state $\mathbf{u}_M$ and right state $\mathbf{u}_R$. We find the intermediate state in the figures as follows: given $\mathbf{u}_R$, follow the two-wave curve backward from $\mathbf{u}_R$ (opposite the direction of the arrows) until you reach a point $\mathbf{u}_M$ in the one-wave curve $\mathscr{W}_1(\mathbf{u}_L)$. The state $\mathbf{u}_M$ so constructed satisfies $\mathbf{u}_R \in \mathscr{W}_2(\mathbf{u}_M)$

and defines the waves in the solution. This procedure is not well defined when $\{\mathbf{u}_L, \mathbf{u}_M, \mathbf{u}_R\}$ form a triple shock:

$$u_M \in \mathscr{H}(\mathbf{u}_L), \quad \mathbf{u}_R \in \mathscr{H}(\mathbf{u}_L), \quad u_R \in \mathscr{H}(\mathbf{u}_M), \tag{3.1}$$

and

$$\sigma(\mathbf{u}_L, \mathbf{u}_M) = \sigma(\mathbf{u}_L, \mathbf{u}_R) = \sigma(\mathbf{u}_M, \mathbf{u}_R). \tag{3.2}$$

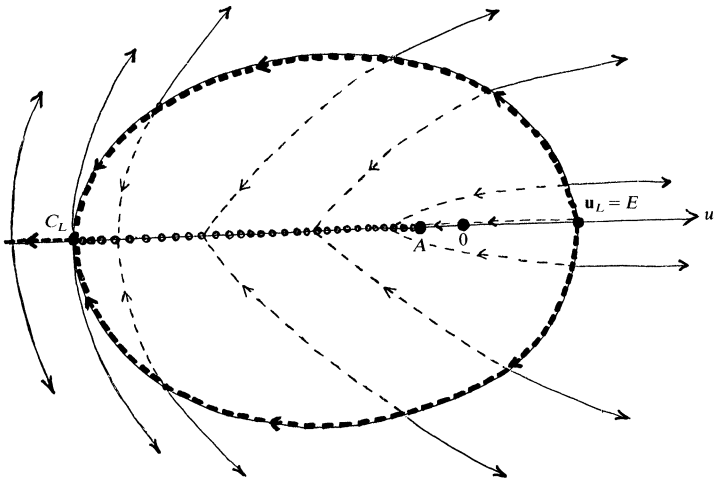

FIG. 7(a). *Riemann problem solution for* $\theta_L = 0$.

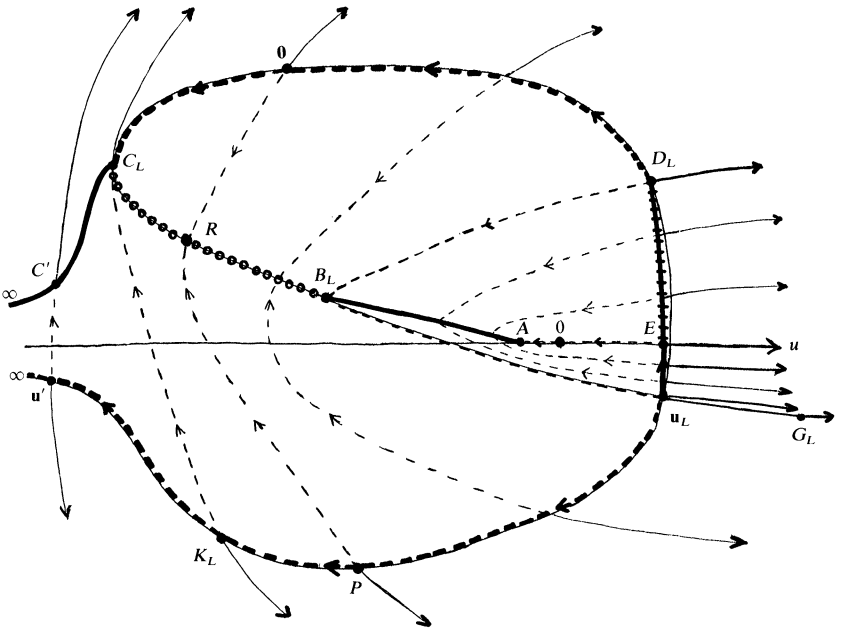

FIG. 7(b). *Riemann problem solution for* $\mathbf{u}_L \in \mathscr{A}_1$.

Triple shocks occur when $\mathbf{u}_R \in \mathscr{S}_c(\mathbf{u}_L)$ or when $\mathbf{u}_R$ is in the triple shock curve (which will be defined in each figure). When the procedure is not well defined, there are two such intermediate states $\mathbf{u}_M$; however, the two solutions obtained are identical in x, t-space because then all shock speeds in the problem are equal. This ensures continuous dependence of the solution on the initial data $\mathbf{u}_L$ and $\mathbf{u}_R$.

We now discuss the solution figure 7(a)–(e) individually.

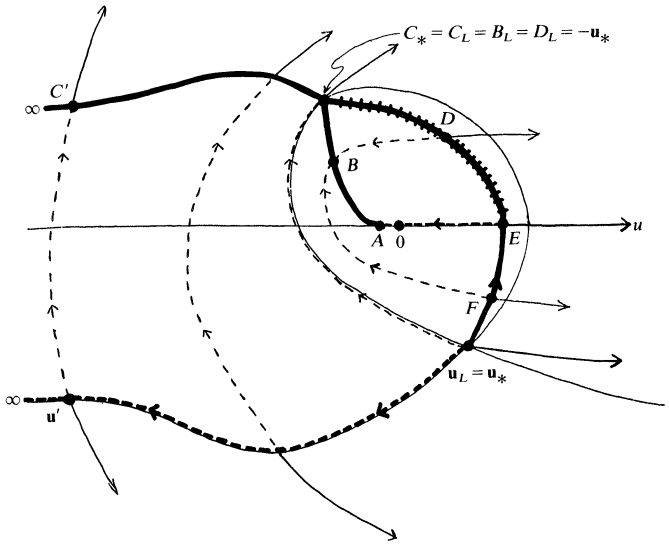

FIG. 7(c). *Riemann problem solution for* $\theta_L = \theta_*$.

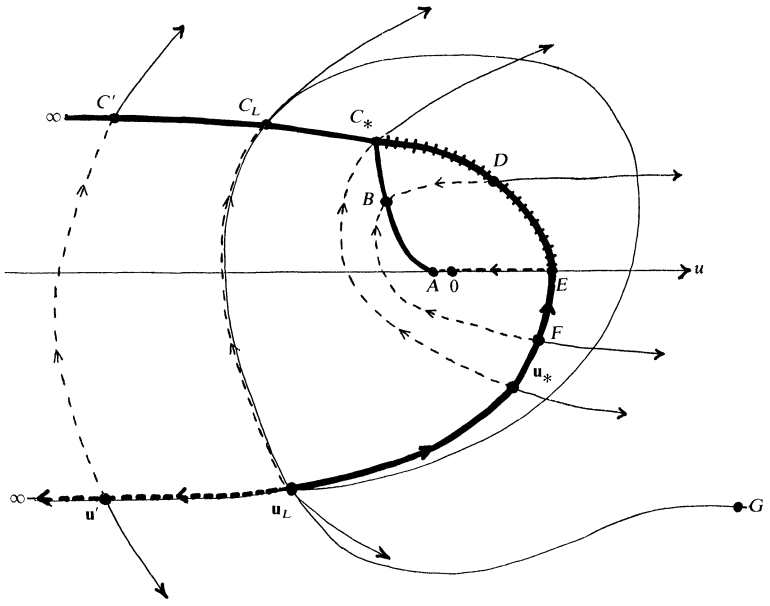

FIG. 7(d). *Riemann problem solution for* $\mathbf{u}_L \in \mathscr{A}_2$.

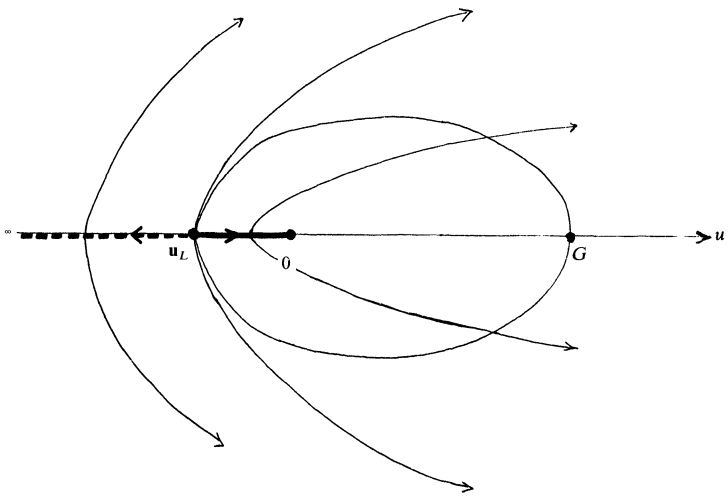

FIG. 7(e). *Riemann problem solution for* $\theta_L = -\pi$.

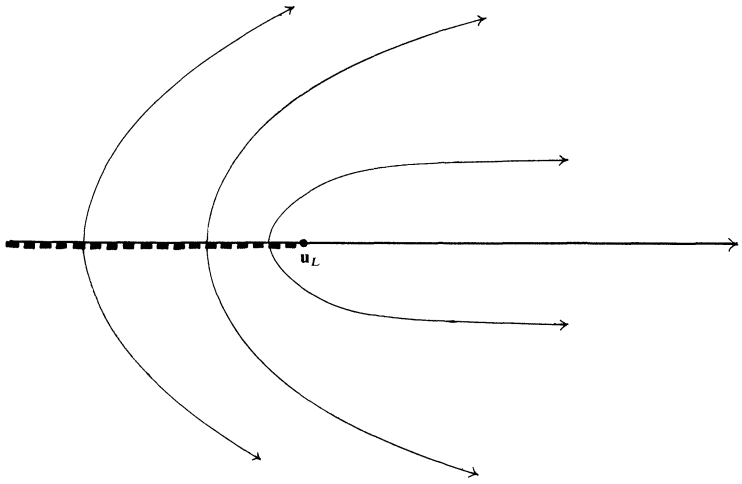

FIG. 7(f). *Riemann problem solution for* $\mathbf{u}_L = \mathbf{0}$.

3.1. Solution for $\theta_L = 0$. In Fig. 7(a), $\mathbf{u}_L \equiv E$ lies on the u-axis to the right of the origin. In this case the Hugoniot locus $\mathscr{H}(\mathbf{u}_L)$ consists of the $\mathbf{u}$-axis together with the ellipse $\mathscr{E}$ depicted. The vertices of $\mathscr{E}$ on the major axis are $\mathbf{u}_L$ and $C_L \equiv -(a/(a-2))\mathbf{u}_L$. Point A is given by

$$A = -\frac{a-2}{a}\mathbf{u}_L. \tag{3.3}$$

Point A is the limit of intersections of $\mathscr{S}_2(\mathbf{u})$ with the u-axis as $\mathbf{u}$ tends to $\mathbf{u}_L$ through states with $v \neq 0$. The solution of the Riemann problem consists of a one-shock with left state $\mathbf{u}_L$ and right state $\mathbf{u}_M \in \mathscr{S}_1(\mathbf{u}_L)$ followed by a two-rarefaction wave if $\mathbf{u}_R$ lies outside $\mathscr{E}$, and followed by a two-shock if $\mathbf{u}_R$ lies inside $\mathscr{E}$. The u-axis between C_L and A is $\mathscr{S}_c(\mathbf{u}_L)$ where triple shocks occur in pairs. In fact, for each $\mathbf{v} \in \mathscr{E}$, $\mathbf{v} \neq \mathbf{u}_L$, there exists a unique $\mathbf{u} \in \mathscr{S}_c(\mathbf{u}_L)$ such that both $\{\mathbf{u}_L, \mathbf{v}, \mathbf{u}\}$ and $\{\mathbf{u}_L, \bar{\mathbf{v}}, \mathbf{u}\}$ are triple shocks of

the same speed. (Here $\bar{\mathbf{v}}$ is the reflection of $\mathbf{v}$ in the u-axis.) Thus for $\mathbf{u}_R \in \mathscr{S}_c(\mathbf{u}_L)$, the solution of the Riemann problem is unambiguous in the x, t-plane.

3.2. Solution for $\theta_* < \theta_L < 0$. In Fig. 7(b), $\mathbf{u}_L$ lies in the sector $\mathscr{A}_1$. The Hugoniot locus $\mathscr{H}(\mathbf{u}_L)$ is depicted by the thin solid curve through $\mathbf{u}_L$. Here

$$\mathscr{S}_1(\mathbf{u}_L) = [\infty K_L \mathbf{u}_L] \cup [D_L C_L], \quad \mathscr{R}_1(\mathbf{u}_L) = [\mathbf{u}_L E], \quad \mathscr{C}_1(\mathbf{u}_L) = [E D_L],$$

and the union of these three curves is the one-wave curve $\mathscr{W}_1(\mathbf{u}_L)$. Moreover,

$$\mathscr{S}_c(\mathbf{u}_L) = [C_L B_L],$$

and the triple shock curve is $[B_L A]$.

For $\mathbf{u}_R$ on either of these latter two curves, triple shocks occur: for $R \in \mathscr{S}_c(\mathbf{u}_L)$ there is a pair of triple shocks $\{\mathbf{u}_L, P, R\}$ and $\{\mathbf{u}_L, Q, R\}$ with all shock speeds being equal; for $R \in [B_L A]$, a single triple shock occurs. Hence, continuous dependence is ensured.

The curve $[C_L C' \infty]$ is the two-boundary curve based on $[K_L \mathbf{u}' \infty]$, and two-*SR*-composite waves occur precisely when $\mathbf{u}_R$ lies "above" $[C_L C' \infty]$ so that $\mathbf{u}_M \in [K_L \mathbf{u}' \infty]$.

The states B_L and D_L satisfy

$$\sigma(\mathbf{u}_L, B_L) = \sigma(\mathbf{u}_L, D_L) = \sigma(D_L, B_L) = \lambda_1(\mathbf{u}_L).$$

The state C_L is the point where $\mathscr{H}(\mathbf{u}_L)$ is tangent to a two-integral curve. (See the Tangency Rule in the Appendix.) This implies that $\sigma(\mathbf{u}_L, C_L) = \lambda_2(C_L)$ and that C_L is in, and marks the end of, the two-boundary curve $[C_L C' \infty]$. This ensures continuous dependence near the point C_L.

For $\mathbf{u}_L$ in Sector $\mathscr{A}_1$, the states B_L, D_L separate the states $\mathbf{u}_L$, C_L on the portion of $\mathscr{H}(\mathbf{u}_L)$ consisting of the closed loop. As θ_L decreases to θ_*, B_L and D_L become coincident with C_L, and so both $\mathscr{S}_c(\mathbf{u}_L)$ and the disconnected portion $[D_L C_L]$ of $\mathscr{S}_1(\mathbf{u}_L)$ disappear. The fact that there exists a point at which $\mathscr{H}(\mathbf{u}_L)$ intersects the one-composite curve $[E D_L]$ characterizes the states in $\mathscr{A}_1$.

3.3. Solution for $\theta_L = \theta_*$. In Fig. 7(c), $\mathbf{u}_L = \mathbf{u}_*$ lies on the line $\theta = \theta_*$. The Hugoniot locus $\mathscr{H}(\mathbf{u}_L)$ is depicted by the thin solid curve through $\mathbf{u}_L$. Here

$$\mathscr{S}_1(\mathbf{u}_L) = [\infty \mathbf{u}' \mathbf{u}_L], \quad \mathscr{R}_1(\mathbf{u}_L) = [\mathbf{u}_L E], \quad \mathscr{C}_1(\mathbf{u}_L) = [E D_L].$$

The union of these three curves is $\mathscr{W}_1(\mathbf{u}_L)$. In this case

$$\mathscr{S}_c(\mathbf{u}_L) = \{C_*\},$$

and the curve $[C_* A]$ is the triple shock curve.

The curve $[C_* C' \infty]$ is the two-boundary curve based on $[\mathbf{u}_L \mathbf{u}' \infty]$, and two-*SR*-composite waves occur precisely when $\mathbf{u}_R$ lies "above" $[C_* C' \infty]$ so that $\mathbf{u}_M \in [\mathbf{u}_L \mathbf{u}' \infty]$. Note that $C_* = -\mathbf{u}_L$ is the point where $\mathscr{H}(\mathbf{u}_L)$ is tangent to a two-rarefaction curve, and also that

$$\sigma(\mathbf{u}_L, C_*) = \lambda_1(\mathbf{u}_L) = \lambda_2(C_*).$$

Thus $\theta = \theta_*$ is the ray where B_L, C_L, and D_L are coincident.

3.4. Solution for $-\pi < \theta_L < \theta_*$. In Fig. 7(d), $\mathbf{u}_L$ lies in sector $\mathscr{A}_2$. The Hugoniot locus $\mathscr{H}(\mathbf{u}_L)$ is depicted by the thin solid curve through $\mathbf{u}_L$. Here

$$\mathscr{S}_1(\mathbf{u}_L) = [\infty \mathbf{u}' \mathbf{u}_L], \quad \mathscr{R}_1(\mathbf{u}_L) = [\mathbf{u}_L F E], \quad \mathscr{C}_1(\mathbf{u}_L) = [E D C_*].$$

The union of these three curves is $\mathscr{W}_1(\mathbf{u}_L)$. In this case

$$\mathscr{S}_c(\mathbf{u}_L) = \varnothing, \tag{3.4}$$

and $[ABC_*]$ is the triple shock curve. Condition (3.4) characterizes the states in $\mathscr{A}_2$.

For $\mathbf{u}_M \in [\mathbf{u}_* EC_*]$, the solution consists of a one-rarefaction wave taking $\mathbf{u}_L$ to $\mathbf{u}_*$ followed by the solution of the Riemann problem $\langle \mathbf{u}_*, \mathbf{u}_R \rangle$ given in § 3.3. The curve $[C_* C_L \infty]$ is the two-boundary curve with base curve $[\infty \mathbf{u}_L \mathbf{u}_*]$, and again two-$SR$-composite waves occur precisely when $\mathbf{u}_R$ lies "above" the curve $[C_* C_L \infty]$ so that $\mathbf{u}_M \in [\infty \mathbf{u}_L \mathbf{u}_*]$.

Note that C_* is the end of the one-composite curve in the sense that there do not exist one-shocks with left states $\mathbf{u} \in [\mathbf{u}_L \mathbf{u}_*]$ that have speed $\lambda_1(\mathbf{u})$.

3.5. Solution for $\theta_L = -\pi$. In Fig. 7(e) $\mathbf{u}_L$ lies on the negative u-axis. The Hugoniot locus consists of the u-axis together with the ellipse $\mathscr{E}$ depicted. The vertices of $\mathscr{E}$ on the major axis are $\mathbf{u}_L$ and $G = -(a/(a-2))\mathbf{u}_L$, and

$$\mathscr{S}_1(\mathbf{u}_L) = [\infty \mathbf{u}_L], \qquad \mathscr{R}_1(\mathbf{u}_L) = [\mathbf{u}_L 0].$$

The union of these two curves is $\mathscr{W}_1(\mathbf{u}_L)$. Here

$$\mathscr{C}_1(\mathbf{u}_L) = \mathscr{S}_c(\mathbf{u}_L) = \varnothing,$$

and the solution of the Riemann problem consists of a one-wave followed by a two-rarefaction wave. The solution for $\mathbf{u}_L = \mathbf{0}$ is similar and given in Fig. 7(f).

4. Justification. The solution of the Riemann problem presented in § 3 is based on the assumptions that the integral curves and Hugoniot loci have the qualitative features discussed in § 2. The relevant features of the integral curves required for our analysis are verified in [3], [17]. The features of $\mathscr{H}(\mathbf{u}_L)$ (including shapes and locations of shock types) have been verified numerically, using an explicit parameterization of $\mathscr{H}(\mathbf{u}_L)$ (see the Appendix). We here present analytical evidence that supports the results of these numerical computations. Note that for $\mathbf{u}_L$ off the u-axis, system (3) in parameter range (5) is strictly hyperbolic and genuinely nonlinear in a neighborhood of $\mathbf{u}_L$, and so the local theory of Lax [11] applies in some neighborhood of $\mathbf{u}_L$. We now discuss the global features of the Hugoniot loci depicted in Fig. 3(a)-(c).

Figure 3(a). In this case $\mathbf{u}_L$ is on the positive u-axis. The Hugoniot locus $\mathscr{H}(\mathbf{u}_L)$ consists of the u-axis together with the ellipse $\mathscr{E}$ given by

$$(a-2)u^2 + 2u_L u + v^2 = a u_L^2,$$

with center $-(1/(a-2))\mathbf{u}_L$. For $\mathbf{u} = (u, 0)$, we have (see the Appendix)

$$\sigma(\mathbf{u}_L, \mathbf{u}) = \tfrac{1}{2}a(u + u_L),$$

$$\{\lambda_1(\mathbf{u}), \lambda_2(\mathbf{u})\} = \{au, u\} \quad \text{and} \quad \{\lambda_1(\mathbf{u}_L), \lambda_2(\mathbf{u}_L)\} = \{au_L, u_L\},$$

which verifies the shock types on the axis, and verifies that the shock type changes at

$$\mathbf{u}_L,\ C_L \equiv -\frac{a}{a-2}\mathbf{u}_L \quad \text{and} \quad A \equiv -\frac{a-2}{a}\mathbf{u}_L.$$

Figure 3(b). In this case $\mathbf{u}_L \in \mathscr{A}_1$. The points B_L, C_L, and D_L are points where a transition in shock type occurs. The existence of the point C_L where $\mathscr{H}(\mathbf{u}_L)$ is tangent to a two-integral curve follows from the geometry of the integral curves. This tangency

at C_L implies (see the Tangency Rule in the Appendix)

$$\lambda_2(C_L) = \sigma(\mathbf{u}_L, C_L).$$

Note also that $\bar{\mathbf{u}}_L$ and $-\mathbf{u}_L$ both lie on $\mathscr{H}(\mathbf{u}_L)$, and

$$\sigma(\mathbf{u}_L, \bar{\mathbf{u}}_L) = u_L, \qquad \sigma(\mathbf{u}_L, -\mathbf{u}_L) = 0.$$

This is obtained from the Midpoint Rule or directly from the Rankine-Hugoniot condition (see the Appendix). Also the speed $\lambda_1(\mathbf{u}_L)$ satisfies

$$0 < \lambda_1(\mathbf{u}_L) = \frac{a+1}{2} u_L - \frac{1}{2}\sqrt{(a-1)^2 u_L^2 + 4v_L^2} < u_L = \sigma(\mathbf{u}_L, \bar{\mathbf{u}}_L),$$

where the left-hand inequality is equivalent to $\mathbf{u} \in \mathscr{A}_1$. Thus, the shock speed $\sigma(\mathbf{u}_L, \bar{\mathbf{u}}_L)$ is larger than $\lambda_1(\mathbf{u}_L)$, but $\sigma(\mathbf{u}_L, -\mathbf{u}_L)$ is smaller than $\lambda_1(\mathbf{u}_L)$; hence, there exists a point $D_L \in \mathscr{H}(\mathbf{u}_L)$ between $\bar{\mathbf{u}}_L$ and $-\mathbf{u}_L$ at which $\sigma(\mathbf{u}_L, D_L) = \lambda_1(\mathbf{u}_L)$. Similarly,

$$\mathbf{u}_0 \equiv \left(\frac{1}{a}\{u_L - \sqrt{(a-1)^2 u_L^2 + a v_L^2}\}, 0\right)$$

is the intersection of $\mathscr{H}(\mathbf{u}_L)$ with the negative u-axis, and satisfies (see Appendix)

$$\sigma(\mathbf{u}_L, \mathbf{u}_0) = u_L.$$

Therefore, there is a point B_L above the u-axis between $-\mathbf{u}_L$ and $\mathbf{u}_0$ at which $\sigma(\mathbf{u}_L, B_L) = \lambda_1(\mathbf{u}_L)$. Consequently, $\{\mathbf{u}_L, B_L, D_L\}$ is a triple shock.

Figure 3(c). In this case $\mathbf{u}_L = \mathbf{u}_*$ is on the ray $\theta = \theta_*$. As θ_L decreases to θ_* in Fig. 3(b), $\mathscr{S}_c(\mathbf{u}_L)$ and the portion $[D_L C_L] \subseteq \mathscr{S}_1(\mathbf{u}_L)$ vanish. In fact,

$$\lambda_1(\mathbf{u}_*) = \sigma(\mathbf{u}_*, -\mathbf{u}_*) = \lambda_2(-\mathbf{u}_*) = 0,$$

indicating that the points B_L and D_L do indeed become coincident with $-\mathbf{u}_*$ as θ_L decreases to θ_*. We also note that $\lambda_2(-\mathbf{u}_*) = \sigma(\mathbf{u}_*, -\mathbf{u}_*)$ implies, by the Tangency Rule, that $\mathscr{H}(\mathbf{u}_*)$ is tangent to a two-integral curve at $-\mathbf{u}_*$, and thus $C_L = -\mathbf{u}_*$.

Appendix. Here we list for reference several properties of the quadratic conservation laws (1) that are helpful in the study of the Riemann problem.

MIDPOINT RULE. *For system* (1), $\mathbf{u}_R \in \mathscr{H}(\mathbf{u}_L)$ *if and only if the line segment joining* $\mathbf{u}_L$ *to* $\mathbf{u}_R$ *is tangent to a p-integral curve at the midpoint of the segment. Moreover, in this case*

$$\sigma(\mathbf{u}_L, \mathbf{u}_R) = \lambda_p\left(\frac{\mathbf{u}_L + \mathbf{u}_R}{2}\right). \tag{A1}$$

Proof. Use the linearity of $\partial \mathbf{f}/\partial \mathbf{u}$ together with the general formula

$$s(\mathbf{u}_R - \mathbf{u}_L) = \mathbf{f}(\mathbf{u}_R) - \mathbf{f}(\mathbf{u}_L) = \left\{\int_0^1 \frac{\partial \mathbf{f}}{\partial \mathbf{u}}(\mathbf{u}_L + \tau(\mathbf{u}_R - \mathbf{u}_L))\, d\tau\right\}(\mathbf{u}_R - \mathbf{u}_L).$$

TRIPLE SHOCK RULE. *For system* (2), *suppose the states* $\mathbf{u}_1, \mathbf{u}_2$, *and* $\mathbf{u}_3$ *satisfy*

$$\mathbf{u}_1 \in \mathscr{H}(\mathbf{u}_2), \quad \mathbf{u}_2 \in \mathscr{H}(\mathbf{u}_3), \quad \mathbf{u}_3 \in \mathscr{H}(\mathbf{u}_1). \tag{A2}$$

Then either $\mathbf{u}_1, \mathbf{u}_2$, *and* $\mathbf{u}_3$ *are collinear or else*

$$\sigma(\mathbf{u}_2, \mathbf{u}_1) = \sigma(\mathbf{u}_3, \mathbf{u}_2) = \sigma(\mathbf{u}_1, \mathbf{u}_3). \tag{A3}$$

Proof. Let $s_{ij} = \sigma(\mathbf{u}_i, \mathbf{u}_j)$. Then

$$s_{21}(\mathbf{u}_2 - \mathbf{u}_1) = \mathbf{f}(\mathbf{u}_2) - \mathbf{f}(\mathbf{u}_1),$$
$$s_{32}(\mathbf{u}_3 - \mathbf{u}_2) = \mathbf{f}(\mathbf{u}_3) - \mathbf{f}(\mathbf{u}_2),$$
$$s_{13}(\mathbf{u}_1 - \mathbf{u}_3) = \mathbf{f}(\mathbf{u}_1) - \mathbf{f}(\mathbf{u}_3).$$

Adding gives

$$(s_{21} - s_{13})(\mathbf{u}_2 - \mathbf{u}_1) + (s_{32} - s_{13})(\mathbf{u}_3 - \mathbf{u}_2) = 0,$$

and the result follows.

TANGENCY RULE. *For system* (3), *assume that* $\mathbf{u}_L \notin \mathcal{H}(\mathbf{0})$. *Then the following statements are equivalent regarding* $\mathbf{u} \in \mathcal{H}(\mathbf{u}_L)$, $\mathbf{u} \neq \mathbf{u}_L$:

(i) $\mathcal{H}(\mathbf{u}_L)$ *is tangent to a p-integral curve at the point* $\mathbf{u}$.

(ii) $\dot{s} = 0$ *at* $\mathbf{u}$. (*The dot denotes differentiation with respect to arclength along* $\mathcal{H}(\mathbf{u}_L)$.)

(iii) $\lambda_p(\mathbf{u}) = \sigma(\mathbf{u}_L, \mathbf{u})$.

Proof. Differentiate

$$s(\mathbf{u} - \mathbf{u}_L) = \mathbf{f}(\mathbf{u}) - \mathbf{f}(\mathbf{u}_L)$$

along $\mathcal{H}(\mathbf{u}_L)$ to obtain

$$\dot{s}(\mathbf{u} - \mathbf{u}_L) + s\dot{\mathbf{u}} = A(\mathbf{u})\dot{\mathbf{u}},$$

or

$$[A(\mathbf{u}) - sI]\dot{\mathbf{u}} = \dot{s}(\mathbf{u} - \mathbf{u}_L). \tag{A4}$$

Suppose $\mathcal{H}(\mathbf{u}_L)$ is tangent to a p-integral curve. Then $\dot{\mathbf{u}}$ is a right eigenvector of A with eigenvalue λ_p so that (A4) becomes

$$(\lambda_p - s)\dot{\mathbf{u}} = \dot{s}(\mathbf{u} - \mathbf{u}_L). \tag{A5}$$

Since $\mathbf{u}_L \notin \mathcal{H}(\mathbf{0})$, the line joining $\mathbf{u}_L$ to $\mathbf{u}$ is not tangent to $\mathcal{H}(\mathbf{u}_L)$ at $\mathbf{u}$. Thus we conclude from (A5) that $\dot{s} = 0$ and $s = \lambda_p$, so that (i)$\Rightarrow$(ii) and (i)$\Rightarrow$(iii). Now suppose (ii). Then (A4) gives that $\dot{\mathbf{u}}$ is an eigenvector and $s = \lambda_p$ for $p = 1$ or 2. Thus (ii)$\Rightarrow$(i) and (ii)$\Rightarrow$(iii). Finally, suppose (iii): $s = \lambda_p(\mathbf{u})$. If $\dot{\mathbf{u}}$ is not parallel to the eigenvector $\mathbf{r}_p$ of $A(\mathbf{u})$ and $\dot{s} \neq 0$, then (A4) implies that $\mathbf{u} - \mathbf{u}_L$ is parallel to $\mathbf{r}_{\hat{p}}$, (the other eigenvector of $A(\mathbf{u})$). However, by the midpoint rule, $\mathbf{u} - \mathbf{u}_L$ is also tangent to an integral curve at $\frac{1}{2}(\mathbf{u}_L + \mathbf{u})$. But this contradicts the fact that if $\mathbf{u}_L \notin \mathcal{H}(\mathbf{0})$, then every line through $\mathbf{u}_L$ is tangent exactly once to an integral curve. Consequently, $\dot{\mathbf{u}}$ is tangent to $\mathbf{r}_p$ at $\mathbf{u}$, and hence $\dot{s} = 0$. Thus (iii)$\Rightarrow$(i) and (iii)$\Rightarrow$(ii).

Eigenvalues and shock speeds. For system (3) with $b = 0$, the eigenvalues are

$$\lambda_{1,2}(\mathbf{u}) = \tfrac{1}{2}\{(a+1)u \pm \sqrt{(a-1)^2u^2 + 4v^2}\}.$$

In addition, if $\mathbf{u}_R \in \mathcal{H}(\mathbf{u}_L)$, then the Rankine–Hugoniot condition gives

$$\sigma(\mathbf{u}_L, \mathbf{u}_R) = \frac{u_R v_R - u_L v_L}{v_R - v_L} \qquad (v_R \neq v_L).$$

Special points on $\mathcal{H}(\mathbf{u}_L)$. For system (3) with $b = 0$,

$$-\mathbf{u}_L \in \mathcal{H}(\mathbf{u}_L) \quad \text{with } \sigma(\mathbf{u}_L, -\mathbf{u}_L) = 0,$$

and

$$\bar{\mathbf{u}}_L \in \mathcal{H}(\mathbf{u}_L) \quad \text{with } \sigma(\mathbf{u}_L, \bar{\mathbf{u}}_L) = u_L.$$

Moreover, $\mathcal{H}(\mathbf{u}_L)$ crosses the u-axis at the points

$$\mathbf{u} \equiv \left(\frac{1}{a} \{ u_L \pm \sqrt{(a-1)^2 u_L^2 + a v_L^2} \}, 0 \right),$$

and for such values of $\mathbf{u}$,

$$\sigma(\mathbf{u}_L, \mathbf{u}) = u_L$$

when $(a-1)^2 u_L^2 + a v_L^2 \geqq 0$.

Parameterization of $\mathcal{H}(\mathbf{u}_L)$. For system (1), the Hugoniot locus $\mathcal{H}(\mathbf{u}_L)$ for $\mathbf{u}_L \notin \mathcal{H}(\mathbf{0})$ is parameterized by the angle φ of the polar coordinate system centered at $\mathbf{u}_L$. Explicitly,

$$u \equiv u(\varphi) = u_L + R \cos \varphi, \qquad v \equiv v(\varphi) = v_L + R \sin \varphi$$

where

$$R \equiv R(\varphi) = -2 \frac{\alpha u_L + \beta v_L}{\alpha \cos \varphi + \beta \sin \varphi},$$

$$\alpha \equiv \alpha(\varphi) = b_1 \sin^2 \varphi + (a_1 - b_2) \sin \varphi \cos \varphi - a_2 \cos^2 \varphi,$$

$$\beta \equiv \beta(\varphi) = c_1 \sin^2 \varphi + (b_1 - c_2) \sin \varphi \cos \varphi - b_2 \cos^2 \varphi.$$

For system (3) with $b = 0$, these become

$$\alpha \equiv (a-1) \sin \varphi \cos \varphi, \qquad \beta \equiv \sin^2 \varphi - \cos^2 \varphi.$$

In particular

$$\lim_{\varphi \to 0^-} |u| = \infty, \qquad \lim_{\varphi \to 0^-} v = \frac{a}{a-2} v_L,$$

$$\lim_{\varphi \to -\pi^+} |u| = \infty, \qquad \lim_{\varphi \to -\pi^+} v = \frac{a}{a-2} v_L.$$

The axes $\mathcal{H}(\mathbf{0})$. For system (1), the Hugoniot locus of the origin consists of the lines determined by the cubic equation

$$-a_2 u^3 + (a_1 - 2b_2) u^2 v + (2b_1 - c_2) u v^2 + c_1 v^3 = 0.$$

For system (3), the equation is

$$-b u^3 + (a-2) u^2 v + 2b u v^2 + v^3 = 0.$$

For $b = 0$, the equation is

$$(a-2) u^2 v + v^3 = 0.$$

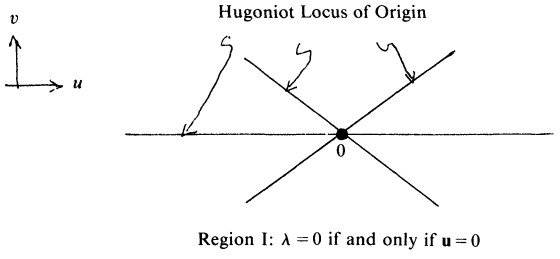

FIG. 8(a). *Relationship between the axes and the lines* $\lambda = 0$ *for Region* I.

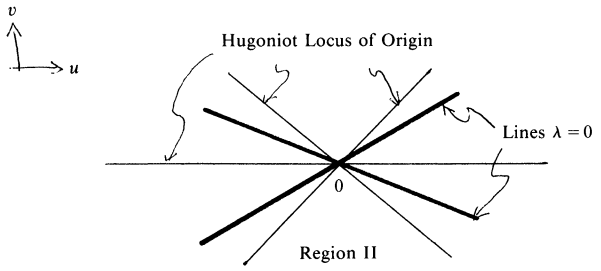

FIG. 8(b). *Relationship between the axes and the lines* $\lambda = 0$ *for Region* II.

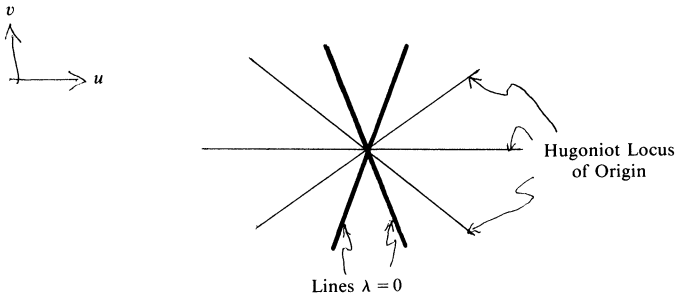

FIG. 8(c). *Relationship between the axes and the lines* $\lambda = 0$ *for Region* III.

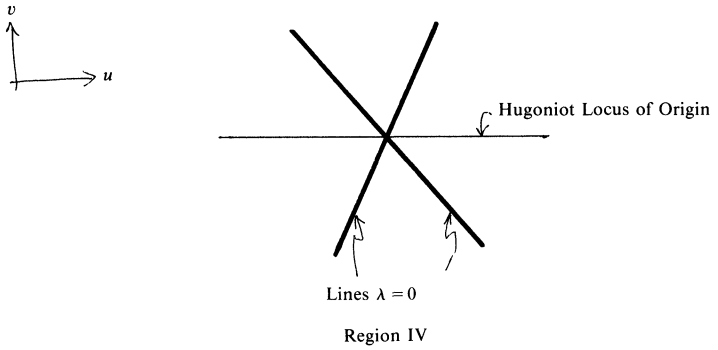

FIG. 8(d). *Relationship between the axes and the lines* $\lambda = 0$ *for Region* IV.

The lines $\lambda = 0$. For system (1), the lines $\lambda = 0$ satisfy the quadratic equation

$$(a_1b_2 - b_1a_2)u^2 + (a_1c_2 - c_1a_2)uv + (b_1c_2 - c_1b_2)v^2 = 0.$$

For system (3), the equation is

$$(a - b^2)u^2 - buv - v^2 = 0.$$

For $b = 0$, the equation is

$$au^2 - v^2 = 0.$$

In particular, for $a > 0$ and $b = 0$, the set of states $\mathbf{u}$ for which $\lambda(\mathbf{u}) = 0$ consists of the two lines through the origin with slopes

$$\frac{v}{u} = \pm\sqrt{a}.$$

The role of the lines $\lambda = 0$ in the classification of the integral curves (see Fig. 8). In Region I, $\lambda = 0$ if and only if $\mathbf{u} = 0$. The boundary between Regions I and II is the set of systems (3) for which the line $\lambda = 0$ coincides with a line in the Hugoniot locus of the origin. Crossing into Region II, this line splits into two lines, and systems in Region II are precisely those that satisfy the condition that the lines $\lambda = 0$ cut through the interiors of the four sectors closest to the u-axis that are determined by the Hugoniot locus of the origin. The boundary between Regions II and III consists of the systems (3) for which the lines $\lambda = 0$ coincide with two lines other than the u-axis in the Hugoniot locus of the origin. And finally, the systems in Region III are characterized by the condition that the lines $\lambda = 0$ cut through the interiors of the two middle sectors determined by the Hugoniot locus of the origin.

REFERENCES

[1] R. ARIS AND N. AMUNDSEN, *Mathematical Methods in Chemical Engineering*, Vol. 2, Prentice-Hall, Englewood Cliffs, NJ, 1973.

[2] R. COURANT AND K. O. FRIEDRICHS, *Supersonic Flow and Shock Waves*, John Wiley, New York, 1948.

[3] G. DARBOUX, *Theorie General des Surfaces*, Chelsea, New York, 1972.

[4] J. GLIMM, *Solutions in the large for nonlinear hyperbolic systems of equations*, Comm. Pure Appl. Math., 18 (1965), pp. 697–715.

[5] F. HELFFERICH AND G. KLEIN, *Multicomponent Chromatography*, Marcel Dekker, New York, 1970.

[6] E. ISAACSON, *Global solution of a Riemann problem for a non-strictly hyperbolic system of conservation laws arising in enhanced oil recovery*, J. Comput. Phys., to appear.

[7] E. ISAACSON AND B. TEMPLE, *Analysis of a singular hyperbolic system of conservation laws*, J. Differential Equations, 65 (1986), pp. 250–268.

[8] ———, *Examples and classification of non-strictly hyperbolic systems of conservation laws*, Abstracts of the AMS, January 1985; presented in the Special Session on "Non-Strictly Hyperbolic Conservation Laws" at the winter meeting of AMS, Anaheim, January 1985.

[9] B. KEYFITZ AND H. KRANZER, *A system of non-strictly hyperbolic conservation laws arising in elasticity theory*, Arch. Rational Mech. Anal., 72 (1980), pp. 219–241.

[10] ———, *The Riemann problem for a class of conservation laws exhibiting a parabolic degeneracy*, J. Differential Equations, 47 (1983), pp. 35–65.

[11] P. D. LAX, *Hyperbolic systems of conservation laws* II, Comm. Pure Appl. Math., 10 (1957), pp. 537–566.

[12] ———, *Shock waves and entropy*, in Contributions to Nonlinear Functional Analysis, E. H. Zarantonello, ed., Academic Press, New York, 1971, pp. 603–634.

[13] R. LEVEQUE AND B. TEMPLE, *Stability of Godunov's method for a class of 2×2 systems of conservation laws*, Trans. Amer. Math. Soc., 288, 1 (1985), pp. 115–123.

[14] T.-P. LIU, *The Riemann problem for general 2×2 conservation laws*, Trans. Amer. Math. Soc., 199 (1974), pp. 89–112.

[15] D. MARCHESIN AND P. J. PAES-LEME, unpublished manuscript.

[16] H. RHEE, R. ARIS, AND N. R. AMUNDSEN, *On the theory of multicomponent chromatography*, Philos. Trans. Roy. Soc. London Ser. A, 267 (1970), pp. 419–455.

[17] D. G. SCHAEFFER AND M. SHEARER, *The classification of 2×2 systems of non-strictly hyperbolic conservation laws, with application to oil recovery*, with Appendix by D. Marchesin, P. J. Paes-Leme, D. G. Schaeffer, and M. Shearer, Comm. Pure Appl. Math., 15 (1987), pp. 141–178.

[18] M. SHEARER, D. G. SCHAEFFER, D. MARCHESIN, AND P. PAES-LEME, *Solution of the Riemann problem for a prototype 2×2 system of non-strictly hyperbolic conservation laws*, Arch Rat. Mech. Anal., 97 (1987), pp. 299–320.

[19] D. SERRE, *Bounded variation solutions for some hyperbolic systems of conservation laws*, J. Differential Equations, to appear.

[20] J. A. SMOLLER, *Shock Waves and Reaction Diffusion Equations*, Springer-Verlag, Berlin, New York, 1980.
[21] B. TEMPLE, *Global solution of the Cauchy problem for a class of* 2×2 *non-strictly hyperbolic conservation laws*, Adv. in Appl. Math., 3 (1982), pp. 335–375.
[22] ———, *Systems of conservation laws with coinciding shock and rarefaction curves*, Contemporary Math., 17 (1983), pp. 143–151.
[23] ———, *Systems of conservation laws with invariant submanifolds*, Trans. Amer. Math. Soc., 280 (1983), pp. 781–795.
[24] M. SHEARER, private communication, 1985.
[25] D. G. SCHAEFFER, private communication, 1985.